REVIEW ARTICLE

Improving radiotherapy planning, delivery accuracy, and normal tissue sparing using cutting edge technologies

Carri K. Glide-Hurst, Indrin J. Chetty

Henry Ford Health Systems, Detroit, MI, USA

ABSTRACT

In the United States, more than half of all new invasive cancers diagnosed are non-small cell lung cancer, with a significant number of these cases presenting at locally advanced stages, resulting in about one-third of all cancer deaths. While the advent of stereotactic ablative radiation therapy (SABR, also known as stereotactic body radiotherapy, or SBRT) for early-staged patients has improved local tumor control to >90%, survival results for locally advanced stage lung cancer remain grim. Significant challenges exist in lung cancer radiation therapy including tumor motion, accurate dose calculation in low density media, limiting dose to nearby organs at risk, and changing anatomy over the treatment course. However, many recent technological advancements have been introduced that can meet these challenges, including four-dimensional computed tomography (4DCT) and volumetric cone-beam computed tomography (CBCT) to enable more accurate target definition and precise tumor localization during radiation, respectively. In addition, advances in dose calculation algorithms have allowed for more accurate dosimetry in heterogeneous media, and intensity modulated and arc delivery techniques can help spare organs at risk. New delivery approaches, such as tumor tracking and gating, offer additional potential for further reducing target margins. Image-guided adaptive radiation therapy (IGART) introduces the potential for individualized plan adaptation based on imaging feedback, including bulky residual disease, tumor progression, and physiological changes that occur during the treatment course. This review provides an overview of the current state of the art technology for lung cancer volume definition, treatment planning, localization, and treatment plan adaptation.

KEYWORDS

Lung cancer; motion management; dose calculation; treatment planning

J Thorac Dis 2014;6(4):303-318. doi: 10.3978/j.issn.2072-1439.2013.11.10

Introduction

In the United States, lung cancer constitutes 56% of all new invasive cancers diagnosed, accounting for ~30% of deaths resulting from all cancers (1). Non-small cell lung cancers (NSCLC) account for 80-85% of all lung cancers (2), with locally advanced, stage III disease representing about 40% of the total cases. The prognosis of these patients, even with aggressive chemoradiation techniques, is quite poor, with 5-year overall survival rates of only 10-15% (3). Given the recent seminal finding that low-dose computed tomography (CT) for lung cancer screening reduces lung cancer mortality ~20% when compared to radiography (4), with widespread acceptance, it may be postulated that lung cancers will be found more frequently, and at earlier stages. For early-stage, medically inoperable NSCLC, stereotactic ablative radiation therapy (SABR, also known as stereotactic body radiotherapy, SBRT) has shown remarkable promise, yielding ~90% local tumor control and, in one study, ~55% overall survival at a time point of three years (5).

Recent retrospective research has shown a dose-effect correlation for lung tumors (6-8), however safe radiation dose escalation is complicated by the close proximity of critical organs, and is further complicated by respiration-induced tumor displacement. However, interim analysis of Radiation Therapy Oncology Group (RTOG) 0617, comparing high dose (74 Gy) versus standard dose (60 Gy) radiation therapy (RT) with and without Cetuximab for Stage III NSCLC patients (9), revealed that the high dose arm did not improve overall survival, with no

Correspondence to: Indrin J. Chetty. Henry Ford Health Systems, Detroit, MI, USA. Email: ichetty1@hfhs.org.

Submitted Sep 12, 2013. Accepted for publication Nov 07, 2013.
Available at www.jthoracdis.com

ISSN: 2072-1439

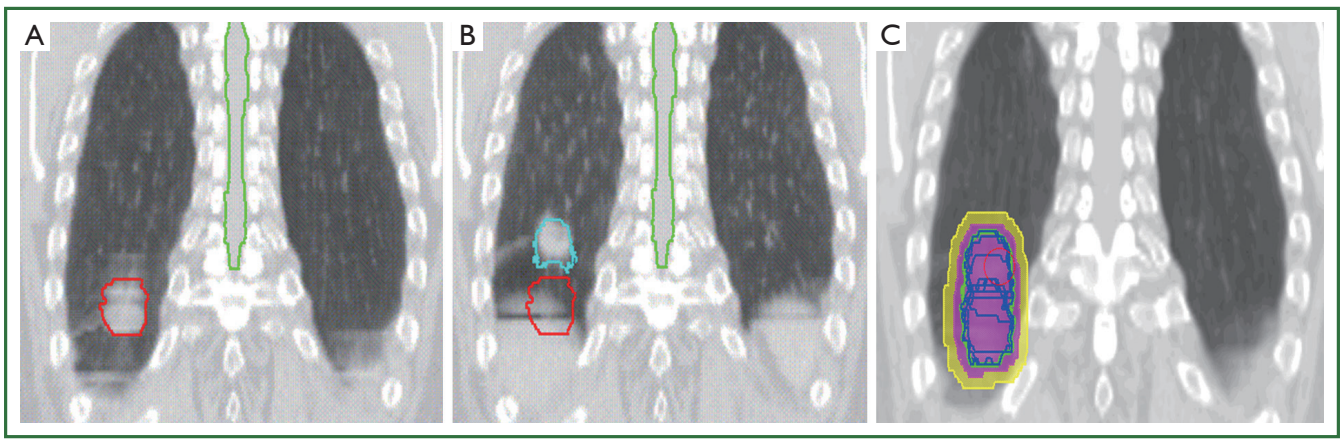

Figure 1. 4DCT images of an early-stage lung cancer patient at end-inhalation (A); end exhalation (B); and contours from all 10 phases of the 4DCT combined (C). Abbreviation: 4DCT, four-dimensional computed tomography.

significant differences in toxicity between treatment arms (10). While mature results are still lacking, the results of this clinical trial prompted a considerable amount of uncertainty in the Radiation Oncology community (11). It has been suggested that requiring the use of technical advances such as image-guided radiation therapy (IGRT), patient-specific dose levels based on nearby organs at risk (i.e., healthy lung tissue and heart), and motion management may be advantageous in future trials (11,12). Motion management is currently recommended on a patient-specific basis for tumor excursions greater than 5 mm in any direction (13). To further facilitate dose escalation and increase local control, considerable effort has been made to characterize patient-specific tumor motion using the tumor (14-16), the organ in which it is embedded (17), implanted fiducial markers (18,19), or another part of the anatomy presumed to be related to tumor motion (i.e., diaphragm or abdomen surface) (20-22).

Advances in imaging, including four-dimensional computed tomography (4DCT) and volumetric cone-beam computed tomography (CBCT) have enabled more accurate target definition and precise tumor localization for both advanced stage lung cancer treatment and SBRT to further support dose escalation efforts while sparing nearby organs at risk. In addition, advances in dose calculation algorithms have allowed for more accurate dosimetry in heterogeneous media, thereby providing a clearer picture of dose distributions. Finally, new delivery approaches, such as tumor tracking or gating, offer additional mechanisms to reduce target margins. This work will provide an overview of the current state of the art for lung cancer volume definition, treatment planning, localization, and treatment plan adaptation.

Internal target volume (ITV)

In 1999, ICRU Report 62 introduced the concept of the "internal margin", which is meant to incorporate uncertainties arising from physiological variations, such as respiratory motion (23). When the internal margin is combined with the clinical target volume, or CTV, the ITV is formed, which represents the "envelope" encompassing tumor movement determined during the simulation 4D-CT acquisition. The internal margin is expanded to form the planning target volume (PTV), which accounts for geometric variation in the CTV due to day-to-day (interfraction) uncertainties in the patient setup. A margin (planning risk volume, PRV) should also be added to an organ-at-risk to account for interfraction variation in the OAR position (23). Margins for the PTV must be designed with an understanding of the random and systematic errors associated with patient setup (24). For locally advanced stage NSCLC, typical margins for the PTV are on the order of 5-10 mm if an ITV is used for motion compensation and daily IGRT is often employed during treatment. In the absence of motion compensation or IGRT, margins should be much larger (10-20 mm) to minimize the chance of missing the target as a result of motion.

The American Association of Physicists in Medicine (AAPM) Task Group Report No. 76 (13) recommends a variety of approaches to account for respiratory motion. One such example is respiratory-correlated or 4DCT (14,25-27), where organ and tumor motion are both inherently provided during different phases of the respiratory cycle, often sampling data over 10-20 breathing cycles. Figure 1A and 1B illustrate the end-inhale and end-exhale phases of respiratory motion, respectively,

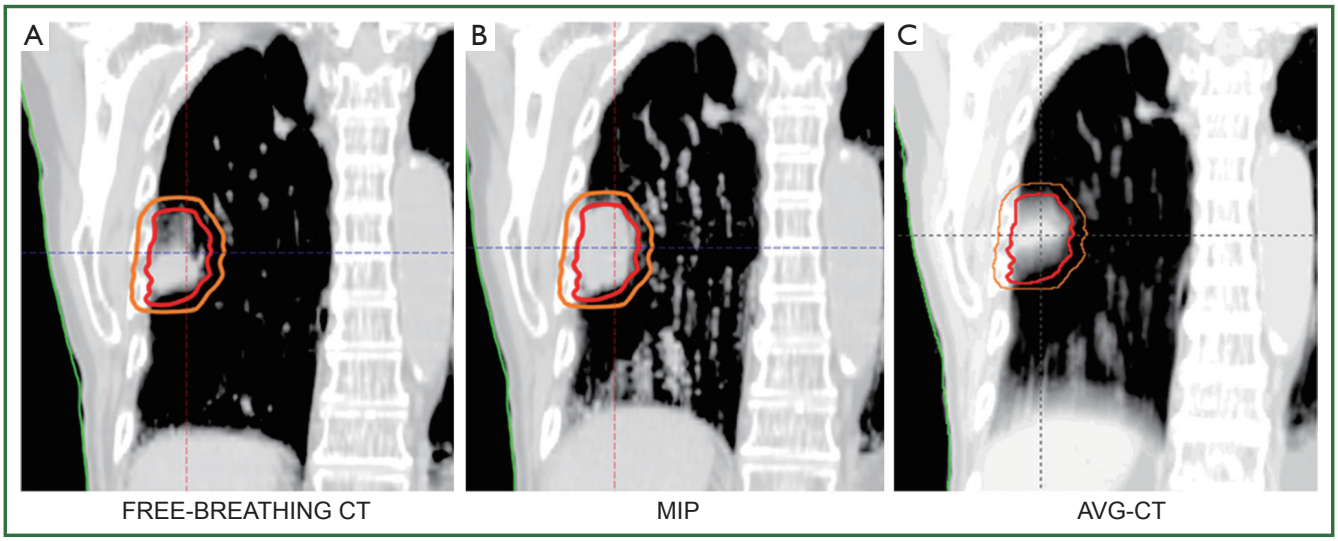

Figure 2. (A) Positional differences between the tumor position on the free-breathing CT; (B) maximum intensity projection (MIP); and (C) AVG-CT, indicating that the FBCT was acquired at an extreme phase of the breathing cycle. Contours show the ITV and PTV. Abbreviations: AVG-CT, average computed tomography; ITV, internal target volume; PTV, planning target volume.

for a highly mobile lung tumor. Tumors can be delineated on all 4DCT phases, and a union can be derived to generate the ITV as shown in Figure 1C. By contrast, conventional free-breathing CTs (FBCTs) are acquired at arbitrary states of the breathing cycle, during which tumors, nearby critical structures, and corresponding tissue densities are not static, as shown in Figure 2. Furthermore, due to the fast acquisition time of FBCT, it is possible to acquire imaging data at an extreme phase of the breathing cycle (i.e., end-inhale or end-exhale). Typically, conventional CT-simulator software employs retrospective temporal (i.e., phase-based) 4DCT sorting into 2-10 different phases, although artifact reduction has been realized through the use of amplitude-based 4DCT binning, particularly for irregular breathing patterns (28). Ten-phase 4DCTs often contain >1,000 CT slices, and may result in reconstruction and sorting artifacts introduced by varied respiratory patterns during a single 4DCT acquisition. This is of particular consequence in lung cancer radiotherapy due to patients presenting with compromised pulmonary function. 4DCT artifacts can lead to discrepancies in target and critical structure delineation, as well as impact the accuracy of dose calculation.

Furthermore, the vast amount of data generated via 4DCT may substantially increase the time needed for image review and target/critical structure delineation. Therefore, a problem arises in how to fully exploit 4DCT data for treatment planning with an emphasis on clinical efficiency without compromising accuracy. To reduce the workload of contouring multiple target volumes in 4DCT, post-processing can be conducted to generate derivative datasets such as the average CT (AVG-CT) and maximum intensity projection (MIP). The AVG-CT data set provides a 3DCT scan with voxels equal to the arithmetic mean of the 4DCT, while the MIP image corresponds to the greatest voxel intensity values throughout the 4DCT. Another commonly used dataset is the mid-ventilation CT scan, corresponding to the specific 4DCT phase with the tumor center of mass closely representing the time-averaged position over the respiratory cycle (29). To further address large 4DCT datasets, several groups have worked toward developing automated contour delineation (30,31), deformable image registration (DIR) techniques (32-34), treatment planning on fewer breathing phases (35), the mid-ventilation phase (29,36), or AVG-CT over the entire breathing cycle (37,38). If 4DCT is not available, end-inspiration and end-exhalation images can be acquired to assess tumor excursion, or the tumor can be observed under fluoroscopy, such as with a conventional simulator.

Dose calculation

Dose calculation accuracy is of paramount importance in the clinical treatment process. The AAPM Report No. 85 (39) on Tissue Inhomogeneity Corrections for Megavoltage (MV) Beams notes that a 5% change in dose may result in a 10% to 20% change in tumor control probability (TCP) at 50%, and 20% to 30% impact on normal tissue complication probabilities

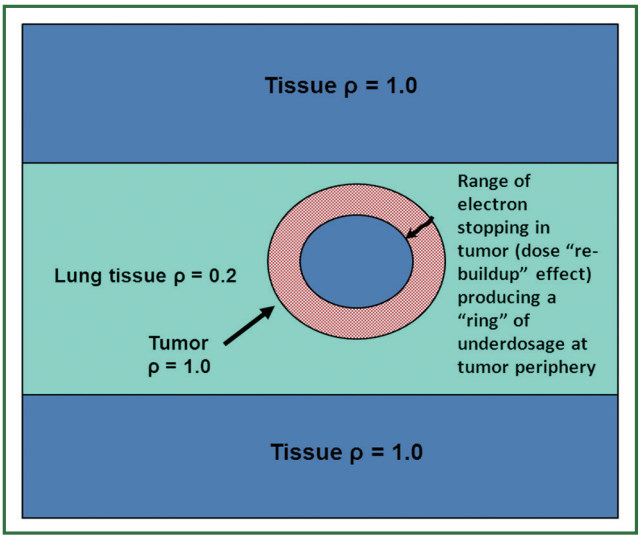

Figure 3. Geometry of an "island-like" lung tumor where electrons scatter laterally into lower density lung tissue, carrying dose away from the tumor. Electrons "stopping" within the tumor deposit dose over a finite range, resulting in an underdosage at the periphery of the tumor. Dose algorithms incorporating 3D scatter corrections, including the effects of electron scattering, must be used to properly characterize dose deposition within the tumor and surrounding healthy lung tissue. Abbreviation: 3D, three-dimensional.

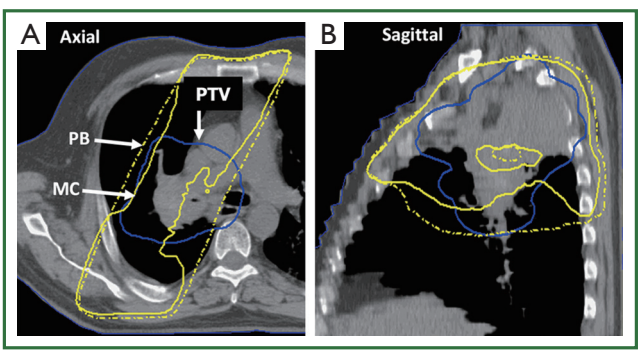

Figure 4. Comparison of 100 % isodose line in a treatment plan for a patient with locally advanced stage non-small cell lung cancer, shown in the axial (A) and sagittal (B) views. Dose calculations performed using a pencil-beam-type algorithm (dashed line) and the Monte Carlo (MC) method (solid line). Significant underdosage of the PTV (solid line) is noted with the MC algorithm using UMPlan (University of Michigan) treatment planning system.

(NTCP). The report further cites two examples where a 7% difference in dose delivered to different groups of patients was discovered by a radiation oncologist through clinical observations (39).

Dosimetric considerations

The presence of low-density lung tissue surrounding thoracic tumors complicates radiation dose computation in lung cancer treatment planning. Conditions of loss of charged-particle equilibrium (CPE) are produced when the field size is reduced such that the lateral ranges of the secondary electrons become comparable to (or greater than) the field size; such conditions occur for larger field sizes in lung than in water-equivalent tissues due to the increased electron range in lung. Under such circumstances, the dose to the target is determined primarily by secondary electron interactions and dose deposition. Because conventional dose algorithms do not explicitly account for transport of secondary electrons, they can be severely limited in accuracy under non-equilibrium conditions. In low density, lung-equivalent tissues, the reduction of dose due to electron scattering in the lung and the "re-buildup" of dose in the tumor at the lung-tumor interface, as electrons begin to stop in the tumor over a finite range, can produce significant underdosage at the tumor periphery (Figure 3). The reduction of dose at the tumor periphery is also exacerbated at higher beam energies, due to the increased electron range. Based on these dosimetric considerations, the RTOG No. 0236 (40) excluded the use of radiation field sizes less than 3.5 cm and restricted the use of beam energies above 10 MV. The article by Reynaert *et al.* (41) and the AAPM Task Group No. 105 (42) provide examples of numerous studies reported on the inaccuracies associated with conventional algorithms for dose calculations in the lung. For lung cancer treatment planning, and especially when dealing with smaller tumors with field sizes <5×5 cm^2, algorithms including three-dimensional (3D) scatter integration such as convolution/superposition, or the Monte Carlo (MC) method are necessary-the latter accounts explicitly for electron transport (43,44).

The AAPM TG Report No. 101 (43) and other articles (45) recommend that pencil-beam algorithms not be utilized for SBRT-based lung dose calculations. The report also states that for the most complex situations, involving small, peripheral lung tumors, surrounded entirely by lung ("island-like" lesions), the MC method is ideal (43). Figure 4 provides a comparison of the 100% isodose line in a treatment plan for a patient with locally advanced stage NSCLC. Dose calculations were performed using a pencil-beam-type algorithm (dashed line) and the MC method (solid line). Whereas the pencil-beam-based calculation shows good dose coverage of the PTV, significant underdosage is noted with the MC algorithm. This example illustrates that PB-based algorithms are relatively insensitive to the presence of low-density lung tissue and do not account for electron scattering within the surrounding lung tissues. Consequently dose to the

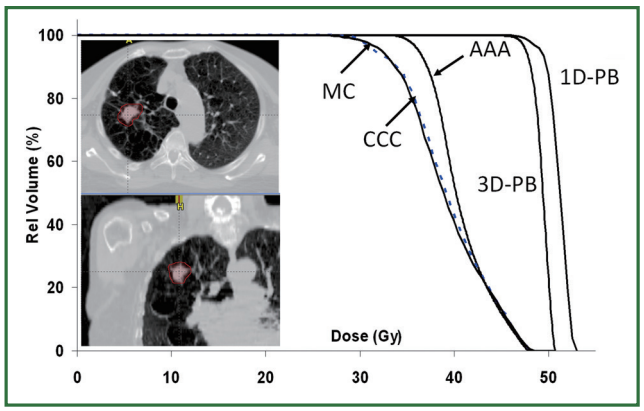

Figure 5. Dose volume histograms (DVHs) for the planning target volume (PTV) for a peripherally located lung tumor with PTV dimensions of ~4.5 cm planned with 6 MV photons. Algorithms include pencil beam-type (1D-PB and 3D-PB), convolution/superposition type (AAA and CCC) and Monte Carlo (MC). All calculations were done using treatment planning systems at the Henry Ford Hospital. Figure adapted from reference 46.

tumor is overestimated using PB algorithms, and the "actual" dose delivered, as properly predicted with the MC method, is much lower.

Figure 5 shows dose volume histograms (DVHs) for the PTV for a peripherally located lung tumor with PTV dimensions of ~4.5 cm planned with six MV photons. The prescription dose was 48 Gy (delivered in four 12 Gy fractions) to the 95% line. The initial 3D conformal (3D-CRT) treatment plan was computed with the 1-D PB algorithm. When re-computed with the convolution/superposition and MC-type algorithms, the "actual" dose to the PTV was much lower than that predicted with the PB algorithm. Both the MC and CCC algorithms show underdosage of the minimum PTV dose of 75% relative to PB (27 *vs.* 48 Gy). Differences in the minimum PTV dose of 25% were noted between MC or CCC and the AAA algorithm; the former which were lower. The substantial differences observed between pencil beam and convolution/superposition or MC-based algorithms for this particular case can be attributed to several factors, including "island-like" geometry (where the tumor is surrounded entirely by lung), relatively small tumor size, and beam arrangements/trajectories. Such conditions amplify the effects of electron scattering and the importance of electron transport; differences are therefore not unexpected.

Table 1 provides the results of a retrospective dose calculation study consisting of 135 patients with early stage NSCLC treated with SBRT (46). As in the example provided in Figure 5, doses were planned initially using a 1D-PB algorithm to a total dose of 48 Gy (in 12 Gy fractions); treatment plans were recomputed using convolution/superposition type and MC-based algorithms. A recently available algorithm, AcurosXB, uses a discrete-ordinates approach to solve the radiation transport equation. It is similar to the MC method but is deterministic in nature. Results in Table 1 show that the convolution/superposition, MC and discrete ordinates algorithms predict differences of ~–10% and ~–20% in the PTV mean and dose to 95% of the volume (D95) values relative to the 1D-PB algorithm. 1D and 3D PB algorithms are generally within 5% agreement. Differences in mean lung dose (MLD) are not significant, in part because the MLD values are low (~3 Gy). These results confirm that pencil-beam type algorithms should be avoided for thoracic cancer treatment planning, particularly for SBRT.

Treatment planning considerations

Beam arrangements for treatment planning of lung cancers can range from simple two-field, parallel opposed fields (e.g., anterior-posterior, opposed, AP/PA) for late stage NSCLC to complex multiple gantry angle, intensity modulated beams for local or locally advanced disease. Beams are shaped with a multileaf collimator (MLC) which enables conformation of radiation to the target. Treatment plans should be designed to minimize dose to surrounding normal organs and thereby limit the risk of treatment toxicity, implying sharp gradients in the dose fall-off outside the target (43). AP/PA fields may be considered with more extensive, centrally located disease to help reduce dose to the unaffected lung volume. The goal in such cases is to produce a homogeneous dose distribution across the treated volume to encompass the extent of the disease. However, AP/PA beams can only be used for cumulative PTV doses in the range of 45-50 Gy (in 1.8-2 Gy per fraction) due to spinal cord tolerance. "Off-cord" fields are required beyond 45-50 Gy. When treating large volumes of lung, it is especially important to design treatment plans that adhere to normal lung tolerance doses. Dose indices, such as V20, V5 and MLD must be closely observed to avoid radiation pneumonitis and other catastrophic consequences (47,48). For treatment planning of local or locally advanced NSCLC, more conformal dose distributions employing multiple beam angles are warranted. Treatment plans can be developed using 3D-CRT or intensity modulated radiation therapy (IMRT) techniques and must include beams from multiple gantry angles (five or more beams), particularly in the context of SBRT (43), to limit normal tissue sequelae, such as skin erythema, which has been observed clinically.

For IMRT-based planning, one must bear in mind the interplay effect, which describes the interplay between a given MLC position and instance of radiation delivery with the

Table 1. Absolute dose values (in Gy) of the PTV mean (Dmean), D95, and MLD early stage NSCLC treatment plans treated with SBRT.

Algorithm	Dmean (Gy)		D95 (Gy)		MLD (Gy)	
	Avg.	Range	Avg.	Range	Avg.	Range
EPL-1D	49.2	46.8-53.6	48.0	38.5-51.8	3.0	0.6-10.3
EPL-3D	47.9	44.3-53.4	45.9	38.7-51.4	3.0	0.4-10.6
AAA	44.7	37.9-52.5	40.8	31.5-48.7	2.8	0.5-9.7
CCC	45.1	37.4-52.8	40.9	30.0-48.6	2.9	0.5-10.1
AcurosXB	44.3	34.2-52.1	39.8	29.8-47.6	3.0	0.5-10.4
MC	45.0	36.2-52.4	40.9	30.5-49.0	2.9	0.5-10.6

Abbreviations: PTV, planning target volume; D95, dose corresponding to 95% of the volume; MLD, mean lung dose. Both average dose and the range are presented for the EPL-1D (pencil beam 1D), EPL-3D (pencil beam 3D), AAA (convolution/superposition type), CCC (convolution/superposition type), AcurosXB (discrete ordinates-type), and Monte Carlo (MC) algorithms. The dose prescription was 48 Gy (in 12 Gy per fraction) to the 95% line, computed initially using the 1D-PB algorithm. The same monitor units and plan parameters as in the 1D-PB plan were used for computation with all other algorithms. All calculations were done using treatment planning systems at the Henry Ford Hospital, adapted from Reference (46).

position of the tumor in the respiratory-induced motion cycle at the same instance (49). For conventional 3D treatment, small dose gradients can be expected and moving anatomy within the treatment field will blur the dose distribution, effectively increasing the beam penumbra (13). Conversely, for IMRT, this effect is more marked due to the interplay between the MLC leaf motions and the target motion perpendicular to the treatment beam. To account for this, the dose deposited for each respiratory phase can be computed by the subset of MLC sequences delivered to that specific phase, rather than by the entire MLC sequence delivered in aggregate. The interplay effect has been evaluated for intra-fraction cumulative dose and while the interplay effect was significant for individual phases, it "washed out" in dose accumulation over ten phases. The interplay effect caused less than 1% discrepancy in the PTV and ITV minimum doses using an energy mapping algorithm (50). Similarly, the interplay effect averages out over 30 or more treatment fractions (49,51). However, in the SBRT setting, where 3-5 dose fractions are delivered, it is not clear how the interplay will impact dose distributions.

Treatment planning for SBRT must be done with an understanding of the dose gradients so as to develop dose distributions with sharp gradients. This is typically achieved using multiple non-overlapping, and non-coplanar beams as necessary, and a MLC with 5 mm or smaller leaf width (43). The dose prescription line can be low (e.g., 80%) with much smaller margins for beam penumbra ("block edge") than conventional radiotherapy; the motivation is to produce a faster dose falloff and thereby improve sparing of surrounding healthy tissues (43). AAPM Task Group No. 101 discourages the use of calculation grid sizes greater than 3 mm for SBRT planning (43).

Recently, volumetric modulated arc therapies (VMAT) have become available for SBRT-based treatments. The delivery of radiation in significantly less time with VMAT is likely to substantially mitigate patient movement on the treatment table as a result of discomfort during a long treatment procedure, and thereby improve delivery quality (52). Another advantage of VMAT is the ability to deliver multiple beams in different directions and preferentially spare neighboring critical structures. However, one must be cognizant of "low-dose" spread with VMAT, which may be higher than IMRT due to the rotational delivery. As such, parameters such as V5 to the healthy lung tissue must be carefully assessed when using VMAT. Nevertheless, comparisons of VMAT and 3DCRT have revealed no early clinical or radiographic changes in the lung post-treatment (53). Also, as with conventional IMRT, VMAT-based plans are subject to the interplay effect, which must be considered depending on the mobility of the tumor and the degree of modulation of the MLC fields.

4D dose accumulation

With widespread 4DCT implementation, a natural progression has been made to estimating the delivered dose during respiration through the use of 4D treatment planning and dose accumulation (32,54,55). Because the tumor and nearby organs at risk change in density and shape during the different phases of respiration, it is advantageous to calculate dose on each, or a subset, of breathing phases, and accumulate the dose to a reference phase. To accomplish this, DIR is necessary to generate the displacement vector field (DVF) between the source and reference images. DVFs describe the voxel-by-voxel correlation across multiple CT sets, and can be used to map the doses deposited during other phases back to the reference phase. The most straightforward, although not efficient, implementation of 4D dose accumulation is to perform a full 4D dose calculation

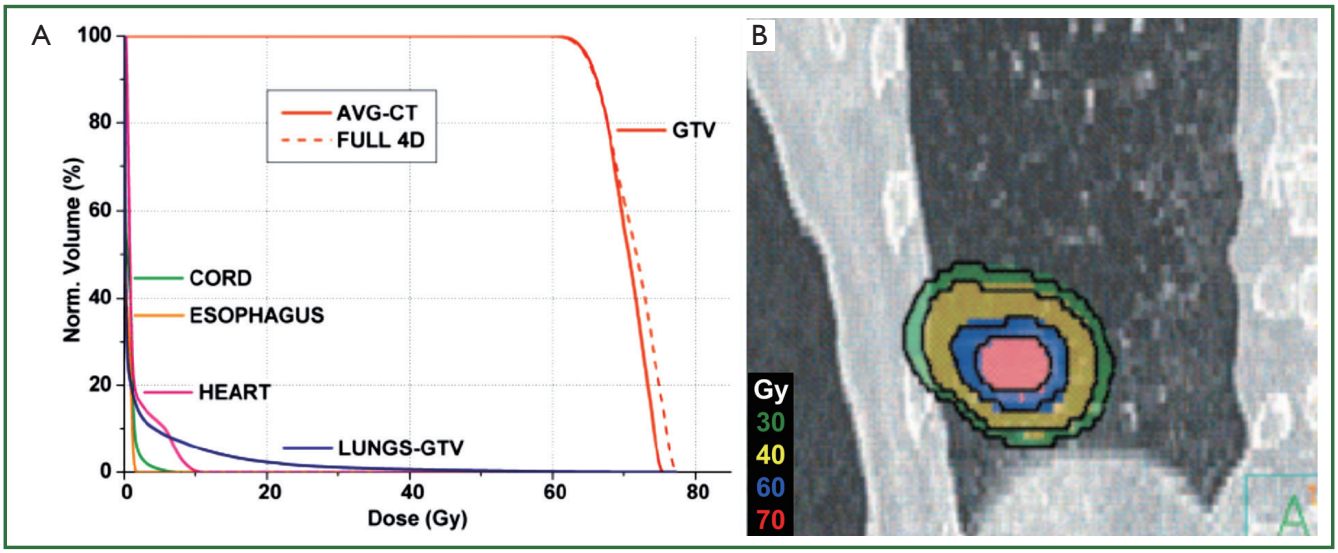

Figure 6. Dose volume histogram (A) and coronal 4DCT data set (B) demonstrating the close association between deformable image registration coupled with full 4D dose summation or using the AVG-CT as an approximation for a patient with 2 cm superior-inferior tumor excursion. Isodose washes represent the AVG-CT approximation while the black isodose lines represent the corresponding full 4D dose summation. Figure adapted from Ref (56). Abbreviations: 4DCT, four-dimensional computed tomography; AVG-CT, average computed tomography; 4D, four-dimensional.

and calculate the weighted average over the breathing course (35). In an effort to simplify 4D dose calculation and computational expense, reduction in datasets have been proposed such as coupling the DVFs with the AVG-CT to estimate cumulative dose (56), using fewer breathing phases (35), or using the midventilation phase (54,57). All of these approaches have revealed close approximations to a full 4D dose accumulation, thereby supporting integration of cumulative dose into clinical treatment planning. For example, in a patient case that was considered to be the worst-case scenario (tumor abutted the diaphragm with ~2 cm of superior-inferior motion), the largest deviation observed between DIR coupled with full 4D dose accumulation or the AVG-CT was 2% for the maximum dose and dose to 1% of the gross target volume (56) as shown in Figure 6.

Another method that has been proposed is to determine the actual energy and mass transferred to that voxel, and then divide the energy by mass to get the dose (termed energy/mass transfer mapping) (58-61). A comparison of direct dose mapping and energy/mass transfer mapping in ten patients with demonstrable tumor excursion revealed similar cumulative doses to the ITV and PTV, although minimum dose differences of up to 11% in the PTV and 4% in the ITV minimum doses were observed between the two dose mapping algorithms with treatment plans computed with AAA (62).

While DIR facilitates cumulative dose estimation, propagated DIR errors will lead to irregularities in automatic contouring, dose warping, and overall dose accumulation. However, verification of DIR is challenging due to the absence of "ground truth". Commonly, visual assessment of the DIR results is conducted, sometimes evaluating propagated contours or the deformed image set (63,64). Others have evaluated DIR performance against physician delineations or noted landmarks (65,66). However, large registration errors are often observed in regions of uniform intensity, and errors estimated by feature-guided evaluation methods may not represent voxel registration accuracy away from those landmarks. Approaches such as evaluating the curl vector (67) or warping images with known DVFs and evaluate the recovered deformations have been implemented (64). Stanley *et al.* benchmarked and evaluated DIR algorithms using patient-specific finite element models (FEM) and a physical deformable phantom (68). Figure 7A shows a programmable deformable phantom that contains a heterogeneous sponge with average density equivalent to lung (Figure 7B) that can be deformed. The modular phantom can be disassembled to insert film or thermoluminescent dosimeters for 4D dose verification.

On-line IGRT

On-line IGRT verifies the target volume and organ at risk locations before daily treatment (inter-fraction) and can also be used to monitor the target during treatment (intra-fraction). Daily IGRT-based setup has been shown to significantly reduce residual errors, and consequently planning margins (69,70). For

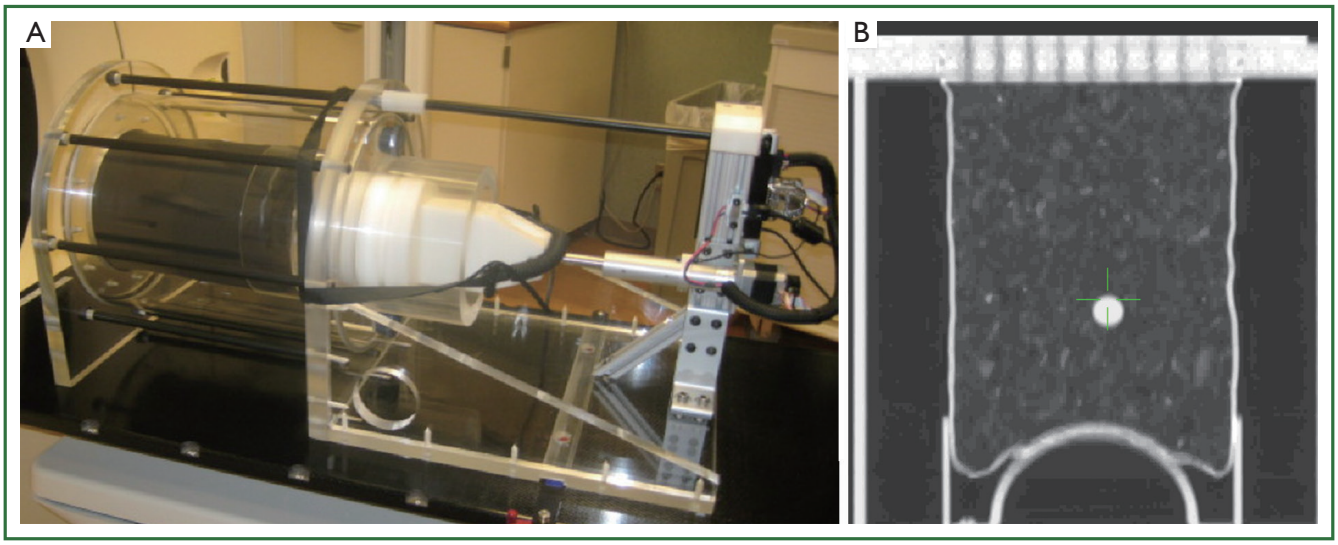

Figure 7. In-house developed deformable lung phantom (A) and coronal cross section (B) showing implanted tumor embedded in the lung material (Courtesy of Hualiang Zhong, Henry Ford Health System).

SBRT-based treatments, where motion management and IGRT are the recommended standard-of-care (43), PTV margins can range from 3-6 mm (69,71-73). On-board imaging can include a kilovoltage (kV) source and flat-panel detector mounted orthogonal to the MV therapy beam axis on the linear accelerator gantry. Image acquisition includes planar radiographic (i.e., kV images), fluoroscopic (cine loops of triggered planar kV images), and volumetric (series of angular projection images reconstructed to generate CBCT datasets (74-78). A chief advantage of kV imaging, particularly CBCT, is the soft tissue visibility, which has been a key component of implementing lung SBRT (70,79,80). Furthermore, because CBCTs are acquired over ~1 minute, the 3D volume represents a time-averaged scan, often indicating the average position of the tumor. Most linear accelerators are also equipped with MV electronic portal imaging devices (EPIDs) mounted at the exit of the treatment beam, which can be used to verify bony landmarks. MV CBCT is also available using an EPID mounted on the treatment beam axis, allowing for volumetric MV imaging.

At Henry Ford Hospital, volumetric CBCT-based imaging is employed to visualize the tumor with respect to organs at risk, for lung SBRT cases. The localization procedure includes setting the patient to tattoos, acquiring a CBCT image, and using automatic image registration tools to align the CBCT to the reference CT. Bony alignment is first verified by the physicist, and manually adjusted if deemed necessary. The physician and physicist then review the registration using soft-tissue window/level and verify that the ITV contour encompasses the lesion. If the lesion falls outside the ITV contour, the physician will manually adjust the registration until the targets are aligned. The image registration is then approved by the physician, and resulting couch corrections are applied. Verification imaging is performed via an orthogonal pair of MV/kV images that are automatically registered to the digitally reconstructed radiograph (DRR). MV/kV matching ensures the proper couch shift has been applied and the patient has not moved between the original CBCT acquisition and treatment. If the registration result is <2 mm/1 degree (not including shifts made for soft tissue matching in the previous step), treatment commences at the CBCT position. Otherwise, another CBCT is performed and the process is repeated.

Ideally, respiratory-correlated CBCT (or 4D-CBCT) would be implemented to mitigate breathing artifacts while providing the tumor mean position, trajectory, and shape over respiration (81). While the feasibility of 4D-CBCT has been demonstrated on different linear accelerators (82,83), scan times can be on the order of four minutes, yielding ~700 projections of data for sorting, and delivering 2-4 cGy/scan depending on area of interest evaluated (81). Another solution that has been integrated into some clinical workflows include a multiple breath-hold CBCT, often called the "stop and go" CBCT (84,85). Here, CBCT acquisition is paused over multiple breath-holds and the resulting datasets are combined into one final reconstruction.

Tracking

Tumor tracking

Lung tumor motion can be measured and monitored using

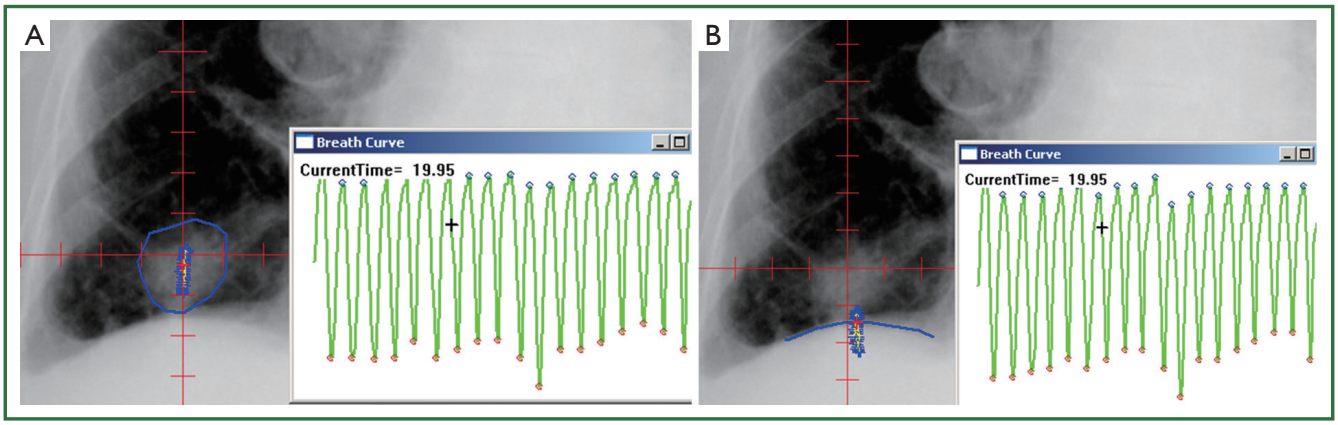

Figure 8. AP fluoroscopy images of an advanced stage lung cancer patient with the tumor (A) and diaphragm (B) tracked using automated in-house software [Courtesy of Jian Liang, William Beaumont Hospital, adapted from Reference (86)].

techniques such as fluoroscopy (15,86), real-time tumor tracking radiotherapy (RT-RT) (18,19), or using implanted fiducials. An example of an in-house analysis program designed to track the tumor and diaphragm in fluoroscopy frames is shown in Figure 8A and B, respectively. Details and validation can be found elsewhere (20,36), but briefly, a region of interest (ROI) is contoured on a single frame, and a template-matching technique using rigid-body registration and nearest-neighbor interpolation propagated the ROI to all other frames. For patients, ROIs can include the tumor or nearby ROI, apex of the diaphragm, or any other anatomy of interest. Centroids of the propagated contours can then be exported to generate the tumor or surrogate trajectories over fluoroscopic frames.

The fluoroscopic real-time tumor-tracking system (RTRT system) (Mitsubishi Electronics Co. Ltd., Tokyo, Japan) uses four sets of diagnostic X-ray systems oriented with the central axis at isocenter to track gold markers implanted at or near moving tumors (15,87-90). 3D marker positioning is determined via a template-matching algorithm applied to the digital images, and if the measured and expected marker positions do not match inside pre-determined tolerances, a machine interlock is asserted. Clinical outcome data suggests similar local control and overall survival rates for RTRT as compared to SBRT without gating (91). One caveat is that significant skin surface doses (29-1,182 mGy/h) have been reported (92).

Another external-internal tumor tracking modality is the Synchrony™ Respiratory Tracking System (Accuray, Inc., Sunnyvale, CA, USA) integrated with the CyberKnife robotic linear accelerator. Briefly, the Synchrony camera array tracks three external LED markers affixed to the patient's chest while orthogonal stereoscopic X-ray images are obtained to localize two to four fiducial markers implanted at or near the tumor (93). Real-time feedback from patient monitoring is used to develop a correspondence model, inferring internal tumor positioning from the external surrogates. The correspondence model predicts tumor position, sends feedback to the robotic linear accelerator, and the robot realigns the beam with the tumor. A soft-tissue tracking algorithm has also been reported that can be used for peripheral tumors (diameter >15 mm) in the lung (94). A few disadvantages include the use of ionizing radiation and the additional margin required to account for deformation (94).

The implantation of electromagnetic transponders [e.g., Calypso wireless transponders (Beacons™) currently part of Varian Medical Systems, Palo Alto, CA] at or near the tumor has been widely implemented in prostate cancer RT (95). Briefly, the system uses an array of AC magnetic coils to generate a resonant response in implanted transponders (8 mm length, 2 mm diameter) subsequently detected using a separate array of receiver coils. Beacons' coordinates are identified on a treatment planning CT, and the offset between the beacons' centroid and intended isocenter is reported. During treatment, the Calypso system continuously monitors and reports the 3D offset between the actual and desired isocenter locations at a frequency of 10 Hz. Transponders have been implanted into canine lungs, although migration and transponder expulsion were challenges for the original beacon design (96,97). As a result, a new anchored beacon was devised under an Investigational Device Exemption (IDE) granted by the FDA, and clinical trials are currently underway (98). While tracking implanted markers within the tumor is optimal, the invasiveness of implantation, increased risk of pneumothorax (99), and potential "dropping" or migration of markers from the implantation location (87) can also be deterrents.

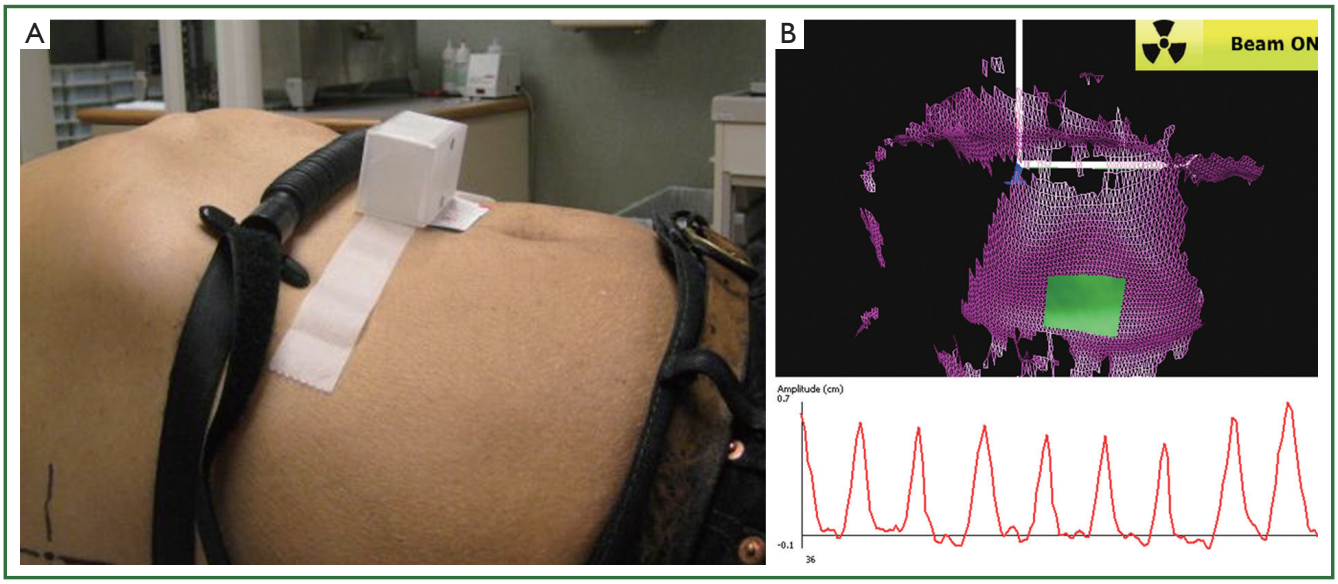

Figure 9. Examples of external surrogates used for patient monitoring. (A) Pneumatic belt placed superiorly of the RPM block; (B) surface images obtained from AlignRT [adapted from Reference (86)]. Abbreviation: RPM, Respiratory Gating System.

External surrogate tracking

External surrogates can infer tumor motion, although they can be limited by the need to verify the relationship with the tumor motion, the potential for external marker placement to affect this correlation (100), and time-dependent characteristics (101). External surrogates of the abdomen can be derived from pressure-sensitive belts, infrared blocks, or surface images. One such example is the Real-Time Position Management Respiratory Gating System (RPM) (Varian Medical Systems, Palo Alto, CA, USA). Briefly, the RPM system uses a plastic block containing two to six markers that reflect infrared light (Figure 9A). These markers are subsequently tracked with an infrared-sensitive charge-coupled device camera, and this video signal is transferred back to the RPM computer. RPM can be used for 4DCT sorting, or coupled with respiratory gating with linear accelerators. Another device that derives an external surrogate includes a pneumatic belt (bellows) (Philips Medical Systems, Cleveland, OH, USA) consisting of a rubber belt that expands and contracts as patients' breathing volumes change (Figure 9A). Changes in the pressure are converted via a transducer to a voltage signal that is then digitized and sent to the CT scanner system for 4DCT sorting. In a simultaneous comparison of bellows and RPM, slight differences in waveform and latency analyses were observed, particularly for low amplitude motions. However, these did not adversely impact image quality or delineations (102). Another example of a pressure sensor is Anzai Medical's small pneumatic sensor.

Video camera-based, 3D imaging systems are available that are used to derive 3D surface images during RT, for example AlignRT (VisionRT Ltd., London, UK) and C-Rad Sentinel™ (C-RAD AB, Uppsala, Sweden). AlignRT uses two or three cameras combined with a projected speckled-light pattern to derive 3D surface images (shown in Figure 9B), whereas C-Rad uses a line scanning mode with a single camera and laser system. Reference datasets can be derived from RT structure sets (i.e., a CT external structure) or from a previously acquired 3D surface acquisition. Rigid body transformations are used by the systems to perform a least square fit to minimize the difference between the planned 3D model of the patient relative to isocenter and the observed surface model of the patient (103). In a study of simultaneous surface imaging and kV fluoroscopy acquisition of three lung cancer patients in the treatment position, most patient fractions studied showed associations between the abdomen and tumor were equivalent or better than those observed between the diaphragm and tumor. Improved internal-to-external associations have been observed when multiple markers or deformed surface images were used as external surrogates (104-106), although these approaches can be computationally expensive and are not currently incorporated into standard clinical practice. One study explored implementing multiple internal surrogates, such as the air content, lung area, lung density, and body area for 4D CT sorting, and found strong agreement with external surrogates recorded by RPM (107).

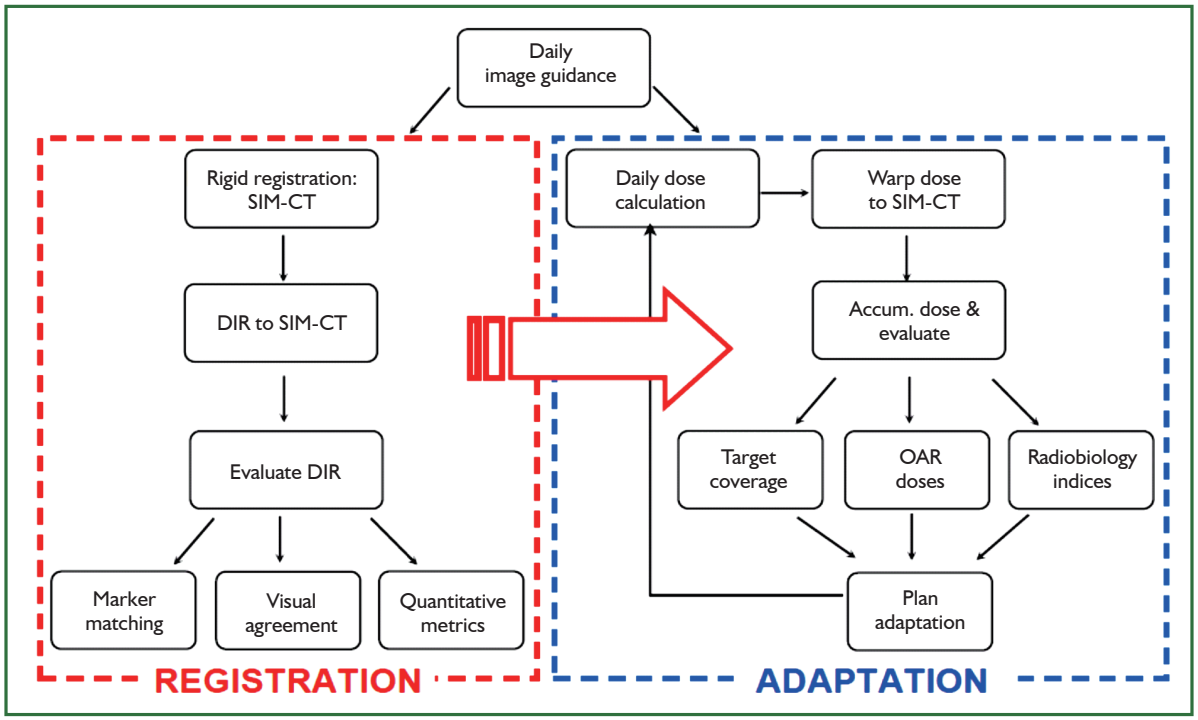

Figure 10. Image-guided adaptive radiation therapy framework developed at Henry Ford Health System. Figure adapted from Ref (120).

Image-guided adaptive radiation therapy (IGART)

While IGRT, such as CBCT, has improved target localization accuracy by providing daily positional information used for online repositioning, daily target and critical structure deformation cannot be fully accounted for using IGRT alone. To combat this, IGART can be implemented. IGART uses patient-specific dynamic/temporal information for potential treatment plan modification during the treatment course (108-110). IGART can address tumor volume and positional changes, as well as other pathologic changes and deformations occurring during the RT treatment course. For lung cancer, inter-fraction baseline variability in lung tumor position, its respiratory trajectory, and normal structures relative to the bony anatomy have been observed (20,36,111-115). Without adjustment, marginal misses can occur. Two cases in point are where a bronchial obstruction is relieved and collapsed lung is re-expanded, resulting in possible tumor shift (116) or in a patient with fluid accumulation in the lungs over the treatment course due to pneumonia (115). Significant reduction in tumor size, particularly for large tumors, has been observed throughout treatment for conventional fractionated radiotherapy of NSCLC (117,118), suggesting that this lung cancer population may benefit most from ART techniques. Conversely, for SBRT, ART has been shown to offer limited value due to the small amount of target volume changes over the shortened time course (119).

To accomplish IGART, a workflow is needed that includes high-quality, temporal volumetric information that is used as a feedback loop in the DIR, dose reconstruction, dose accumulation, and plan adaptation processes (120) as shown in Figure 10. An offline IGART framework has been implemented consisting of a closed-loop system incorporating feedback from updated patient geometry (i.e., CBCTs) and anatomical information to recompute dose and determine the actual dose delivered to the target and surrounding healthy tissues (120). Similar concepts have been proposed previously (108,121), although a unique feature of the presented framework is that it includes a systematic validation of the DIR algorithm and dose accumulation techniques.

On-line plan re-optimization using an "anatomy of the day" approach has also been implemented. Li *et al.* have developed new IMRT plans using daily IGRT images using a two-step process: segment aperture morphing (SAM), to correct for target deformation/translation using the MLC, and segment weight optimization (SWO), to determine the optimal MU for each segment (122). Full plan re-optimization can be accomplished in ~10 minutes. While this would be challenging to implement

in the clinic, on-line IGART is becoming more realistic due to recent advances in computing such as implementing the graphics processing unit (GPU) (123-125), which has reduced online optimization time from minutes down to seconds.

A prospective, randomized, multi-institutional clinical trial is currently underway to incorporate a during-RT PET/CT-adapted boost for patients with large lung tumors that may potentially benefit from dose escalation (12). In this manner, individualized ART will be performed for patients with inoperable or unresectable stage III NSCLC, a population in which overall prognosis currently remains quite poor despite advances in RT techniques including IMRT and IGRT. Controlled clinical trials such as this will help streamline IGART approaches into clinical practice.

Conclusions and future directions

Lung cancer RT is complicated by tumor motion, challenges of accurate dose calculation in low density media, and changing anatomy over the treatment course, in addition to radiobiologic and individual patient-response-specific issues. As tumor localization improves, whether via high quality daily IGRT images or tumor tracking, margin reduction and further dose escalation is possible. Furthermore, dose calculation accuracy has substantially improved in recent years, including the ability to incorporate 3D scatter and implement MC for modeling electron transport, and these algorithms are now available in the clinic. 4DCT and DIR have made dose accumulation and IGART possible, and advances in computational speed will continue to make on-line IGART more clinically plausible over the treatment course.

Some promising new techniques currently being evaluated include incorporating biological feedback into treatment planning, such as dynamic contrast-enhanced MRI (DCE-MRI) as an early indicator of treatment response and perfusion changes (126,127), exploring the role of nanoparticles in lung cancer (128), and exploiting radiosensitizers during RT (129). Finding new ways to assess dose response, normal tissue sparing, and identify opportunities for dose escalation, particularly for advanced stage lung cancer patients, is advantageous.

Acknowledgements

Disclosure: HFHS, Department of Radiation Oncology receives grant funding from the NIH/NCI and industrial partners, Varian Medical Systems and Philips Health Care.

References

1. Jemal A, Siegel R, Ward E, et al. Cancer statistics, 2008. CA Cancer J Clin 2008;58:71-96.
2. Kong FM, Chetty IJ. Advancements in radiation therapy for medically inoperable early stage non-small cell lung cancer: leading article. Current Medical Literature, Respiratory Medicine 2006;20:57-65.
3. Hayman JA, Martel MK, Ten Haken RK, et al. Dose escalation in non-small-cell lung cancer using three-dimensional conformal radiation therapy: update of a phase I trial. J Clin Oncol 2001;19:127-36.
4. National Lung Screening Trial Research Team, Aberle DR, Adams AM, et al. Reduced lung-cancer mortality with low-dose computed tomographic screening. N Engl J Med 2011;365:395-409.
5. Timmerman R, Paulus R, Galvin J, et al. Stereotactic body radiation therapy for inoperable early stage lung cancer. JAMA 2010;303:1070-6.
6. Kong FM, Ten Haken RK, Schipper MJ, et al. High-dose radiation improved local tumor control and overall survival in patients with inoperable/unresectable non-small-cell lung cancer: long-term results of a radiation dose escalation study. Int J Radiat Oncol Biol Phys 2005;63:324-33.
7. Movsas B, Moughan J, Swann S, et al. Back to B.E.D. predictors of outcome in RTOG non-operative non-small cell lung cancer (NSCLC) trials. Int J Radiat Oncol Biol Phys 2005;63:S230-231.
8. Wang L, Correa CR, Zhao L, et al. The effect of radiation dose and chemotherapy on overall survival in 237 patients with Stage III non-small-cell lung cancer. Int J Radiat Oncol Biol Phys 2009;73:1383-90.
9. Bradley J. Radiation Therapy Oncology Group (RTOG 0617): A randomized phase III comparison of standard dose (60Gy) versus high-dose (74Gy) conformal radiotherapy with concurrent and consolidation carboplatin/ paclitaxel in patients with stage IIIA/IIIB non-small cell lung cancer. Available online: http://www.rtog.org/ClinicalTrials/ProtocolTable/StudyDetails.aspx?study=0617
10. Bradley J, Paulus R, Komaki R, et al. A randomized phase III comparison of standard-dose (60 Gy) versus high-dose (74 Gy) conformal chemoradiotherapy+/-cetuximab for stage IIIA/IIIB non-small cell lung cancer: preliminary findings on radiation dose in RTOG 0617. 53rd Annual Meeting of the American Society of Radiation Oncology 2011:2-6.
11. Cox JD. Are the results of RTOG 0617 mysterious? Int J Radiat Oncol Biol Phys 2012;82:1042-4. Available online: http://dx.doi.org/10.1016/j.ijrobp.2011.12.032
12. RTOG 1106/ACRIN 6697, randomized phase II trial of individualized adaptive radiotherapy using during-treatment FDG-PET/CT and modern technology in locally advanced non-small cell lung cancer (NSCLC). Available online: http://www.rtog.org/ClinicalTrials/, (2012).
13. Keall PJ, Mageras GS, Balter JM, et al. The management of respiratory motion in radiation oncology report of AAPM Task Group 76. Med Phys 2006;33:3874-900.
14. Mageras GS, Pevsner A, Yorke ED, et al. Measurement of lung tumor motion using respiration-correlated CT. Int J Radiat Oncol Biol Phys 2004;60:933-41.
15. Seppenwoolde Y, Shirato H, Kitamura K, et al. Precise and real-time measurement of 3D tumor motion in lung due to breathing and heartbeat,

measured during radiotherapy. Int J Radiat Oncol Biol Phys 2002;53:822-34.
16. Liu HH, Balter P, Tutt T, et al. Assessing respiration-induced tumor motion and internal target volume using four-dimensional computed tomography for radiotherapy of lung cancer. Int J Radiat Oncol Biol Phys 2007;68:531-40.
17. Davies SC, Hill AL, Holmes RB, et al. Ultrasound quantitation of respiratory organ motion in the upper abdomen. Br J Radiol 1994;67:1096-102.
18. Shimizu S, Shirato H, Ogura S, et al. Detection of lung tumor movement in real-time tumor-tracking radiotherapy. Int J Radiat Oncol Biol Phys 2001;51:304-10.
19. Shirato H, Shimizu S, Kunieda T, et al. Physical aspects of a real-time tumor-tracking system for gated radiotherapy. Int J Radiat Oncol Biol Phys 2000;48:1187-95.
20. Hugo G, Vargas C, Liang J, et al. Changes in the respiratory pattern during radiotherapy for cancer in the lung. Radiother Oncol 2006;78:326-31.
21. Mageras GS, Yorke E, Rosenzweig K, et al. Fluoroscopic evaluation of diaphragmatic motion reduction with a respiratory gated radiotherapy system. J Appl Clin Med Phys 2001;2:191-200.
22. Juhler Nøttrup T, Korreman SS, Pedersen AN, et al. Intra- and interfraction breathing variations during curative radiotherapy for lung cancer. Radiother Oncol 2007;84:40-8.
23. ICRU report 62. Prescribing, recording, and reporting photon beam therapy (Supplement to ICRU report 50), (International Commission on Radiation Units and Measurements, Bethesda, MD, 1999).
24. van Herk M, Remeijer P, Rasch C, et al. The probability of correct target dosage: dose-population histograms for deriving treatment margins in radiotherapy. Int J Radiat Oncol Biol Phys 2000;47:1121-35.
25. Keall PJ, Starkschall G, Shukla H, et al. Acquiring 4D thoracic CT scans using a multislice helical method. Phys Med Biol 2004;49:2053-67.
26. Vedam SS, Keall PJ, Kini VR, et al. Acquiring a four-dimensional computed tomography dataset using an external respiratory signal. Phys Med Biol 2003;48:45-62.
27. Ford EC, Mageras GS, Yorke E, et al. Respiration-correlated spiral CT: a method of measuring respiratory-induced anatomic motion for radiation treatment planning. Med Phys 2003;30:88-97.
28. Wink N, Panknin C, Solberg TD. Phase versus amplitude sorting of 4D-CT data. J Appl Clin Med Phys 2006;7:77-85.
29. Wolthaus JW, Schneider C, Sonke JJ, et al. Mid-ventilation CT scan construction from four-dimensional respiration-correlated CT scans for radiotherapy planning of lung cancer patients. Int J Radiat Oncol Biol Phys 2006;65:1560-71.
30. Zhang T, Chi Y, Meldolesi E, et al. Automatic delineation of on-line head-and-neck computed tomography images: toward on-line adaptive radiotherapy. Int J Radiat Oncol Biol Phys 2007;68:522-30.
31. Rietzel E, Chen GT, Choi NC, et al. Four-dimensional image-based treatment planning: Target volume segmentation and dose calculation in the presence of respiratory motion. Int J Radiat Oncol Biol Phys 2005;61:1535-50.
32. Flampouri S, Jiang SB, Sharp GC, et al. Estimation of the delivered patient dose in lung IMRT treatment based on deformable registration of 4D-CT data and Monte Carlo simulations. Phys Med Biol 2006;51:2763-79.
33. Keall PJ, Siebers JV, Joshi S, et al. Monte Carlo as a four-dimensional radiotherapy treatment-planning tool to account for respiratory motion. Phys Med Biol 2004;49:3639-48.
34. Orban de Xivry J, Janssens G, Bosmans G, et al. Tumour delineation and cumulative dose computation in radiotherapy based on deformable registration of respiratory correlated CT images of lung cancer patients. Radiother Oncol 2007;85:232-8.
35. Rosu M, Balter JM, Chetty IJ, et al. How extensive of a 4D dataset is needed to estimate cumulative dose distribution plan evaluation metrics in conformal lung therapy? Med Phys 2007;34:233-45.
36. Hugo GD, Yan D, Liang J. Population and patient-specific target margins for 4D adaptive radiotherapy to account for intra- and inter-fraction variation in lung tumour position. Phys Med Biol 2007;52:257-74.
37. Admiraal MA, Schuring D, Hurkmans CW. Dose calculations accounting for breathing motion in stereotactic lung radiotherapy based on 4D-CT and the internal target volume. Radiother Oncol 2008;86:55-60.
38. Soofi W, Starkschall G, Britton K, et al. Determination of an optimal organ set to implement deformations to support four-dimensional dose calculations in radiation therapy planning. J Appl Clin Med Phys 2008;9:2794.
39. Papanikolaou N, Battista J, Boyer A, et al. AAPM Report No. 85: Tissue inhomogeneity corrections for megavoltage photon beams. AAPM Report No. 85. Medical Physics Publishing, Madison, WI, 2004:1-135.
40. Radiation Therapy Oncology Group. RTOG 0236: a phase II trial of stereotactic body radiation therapy (SBRT) in the treatment of patients with medically inoperable stage i/ii non-small cell lung cancer. 2005. Available online: http://www.rtog.org/ClinicalTrials/
41. Reynaert N, van der Marck SC, Schaart DR, et al. Monte Carlo treatment planning for photon and electron beams. Rad Phys Chem 2007;76:643-86.
42. Chetty IJ, Curran B, Cygler JE, et al. Report of the AAPM Task Group No. 105: Issues associated with clinical implementation of Monte Carlo-based photon and electron external beam treatment planning. Med Phys 2007;34:4818-53.
43. Benedict SH, Yenice KM, Followill D, et al. Stereotactic body radiation therapy: the report of AAPM Task Group 101. Med Phys 2010;37:4078-101.
44. Das IJ, Ding GX, Ahnesjö A. Small fields: nonequilibrium radiation dosimetry. Med Phys 2008;35:206-15.
45. Fragoso M, Wen N, Kumar S, et al. Dosimetric verification and clinical evaluation of a new commercially available Monte Carlo-based dose algorithm for application in stereotactic body radiation therapy (SBRT) treatment planning. Phys Med Biol 2010;55:4445-64.
46. Chetty IJ, Devpura S, Liu D, et al. Correlation of dose computed using different algorithms with local control following stereotactic ablative radiotherapy (SABR)-based treatment of non-small-cell lung cancer. Radiotherapy and Oncology 2013;109:498-504.
47. Allen AM, Czerminska M, Janne PA, et al. Fatal pneumonitis associated

with intensity-modulated radiation therapy for mesothelioma. Int J Radiat Oncol Biol Phys 2006;65:640-5.
48. Marks LB, Bentzen SM, Deasy JO, et al. Radiation dose-volume effects in the lung. Int J Radiat Oncol Biol Phys 2010;76:S70-6.
49. Bortfeld T, Jokivarsi K, Goitein M, et al. Effects of intra-fraction motion on IMRT dose delivery: statistical analysis and simulation. Phys Med Biol 2002;47:2203-20.
50. Li H, Zhong H, Kim J, et al. Investigation of the interplay effect between MLC and lung tumor motions using 4DCT and RPM profile data. Med Phys 2011;38:3692.
51. Yu CX, Jaffray DA, Wong JW. The effects of intra-fraction organ motion on the delivery of dynamic intensity modulation. Phys Med Biol 1998;43:91-104.
52. Matuszak MM, Yan D, Grills I, et al. Clinical applications of volumetric modulated arc therapy. Int J Radiat Oncol Biol Phys 2010;77:608-16.
53. Palma DA, Senan S, Haasbeek CJ, et al. Radiological and clinical pneumonitis after stereotactic lung radiotherapy: a matched analysis of three-dimensional conformal and volumetric-modulated arc therapy techniques. Int J Radiat Oncol Biol Phys 2011;80:506-13.
54. Guckenberger M, Wilbert J, Krieger T, et al. Four-dimensional treatment planning for stereotactic body radiotherapy. Int J Radiat Oncol Biol Phys 2007;69:276-85.
55. Hugo GD, Campbell J, Zhang T, et al. Cumulative lung dose for several motion management strategies as a function of pretreatment patient parameters. Int J Radiat Oncol Biol Phys 2009;74:593-601.
56. Glide-Hurst CK, Hugo GD, Liang J, et al. A simplified method of four-dimensional dose accumulation using the mean patient density representation. Med Phys 2008;35:5269-77.
57. Wolthaus JWH, Schneider C, Sonke JJ, et al. Mid-ventilation CT scan construction from four-dimensional respiration-correlated CT scans for radiotherapy planning of lung cancer patients. Int J Radiat Oncol Biol Phys 2006;65:1560-71. Available online: http://dx.doi.org/10.1016/j.ijrobp.2006.04.031
58. Zhong H, Siebers JV. Monte Carlo dose mapping on deforming anatomy. Phys Med Biol 2009;54:5815-30.
59. Zhong H, Weiss E, Siebers JV. Assessment of dose reconstruction errors in image-guided radiation therapy. Phys Med Biol 2008;53:719-36.
60. Heath E, Seuntjens J. A direct voxel tracking method for four-dimensional Monte Carlo dose calculations in deforming anatomy. Med Phys 2006;33:434-45.
61. Heath E, Tessier F, Kawrakow I. Investigation of voxel warping and energy mapping approaches for fast 4D Monte Carlo dose calculations in deformed geometries using VMC++. Phys Med Biol 2011;56:5187-202.
62. Li HS, Zhong H, Kim J, et al. Direct dose mapping versus energy/mass transfer mapping for 4D dose accumulation: fundamental differences and dosimetric consequences. Phys Med Biol 2014;59:173-88.
63. Rueckert D, Sonoda LI, Hayes C, et al. Nonrigid registration using free-form deformations: application to breast MR images. IEEE Trans Med Imaging 1999;18:712-21.
64. Lu W, Chen ML, Olivera GH, et al. Fast free-form deformable registration via calculus of variations. Phys Med Biol 2004;49:3067-87.
65. Brock KK. Results of a multi-institution deformable registration accuracy study (MIDRAS). Int J Radiat Oncol Biol Phys 2010;76:583-96.
66. Hardcastle N, Tomé WA, Cannon DM, et al. A multi-institution evaluation of deformable image registration algorithms for automatic organ delineation in adaptive head and neck radiotherapy. Radiat Oncol 2012;7:90.
67. Schreibmann E, Pantalone P, Waller A, et al. A measure to evaluate deformable registration fields in clinical settings. J Appl Clin Med Phys 2012;13:3829.
68. Stanley N, Glide-Hurst C, Kim J, et al. Using patient-specific phantoms to evaluate deformable image registration algorithms for adaptive radiation therapy. J Appl Clin Med Phys 2013;14:4363.
69. Bissonnette JP, Purdie T, Sharpe M, et al. Image-guided stereotactic lung radiation therapy. Radiat Oncol 2005;76:S15-S16.
70. Grills IS, Hugo G, Kestin LL, et al. Image-guided radiotherapy via daily online cone-beam CT substantially reduces margin requirements for stereotactic lung radiotherapy. Int J Radiat Oncol Biol Phys 2008;70:1045-56.
71. Shah C, Grills IS, Kestin LL, et al. Intrafraction Variation of Mean Tumor Position During Image-guided Hypofractionated Stereotactic Body Radiotherapy for Lung Cancer. Int J Radiat Oncol Biol Phys 2012;82:1636-41.
72. Slotman BJ, Lagerwaard FJ, Senan S. 4D imaging for target definition in stereotactic radiotherapy for lung cancer. Acta Oncol 2006;45:966-72.
73. Timmerman R, Abdulrahman R, Kavanagh BD, et al. Lung cancer: a model for implementing stereotactic body radiation therapy into practice. Front Radiat Ther Oncol 2007;40:368-85.
74. Jin JY, Ren L, Liu Q, et al. Combining scatter reduction and correction to improve image quality in cone-beam computed tomography (CBCT). Med Phys 2010;37:5634-44.
75. Wang J, Li T, Xing L. Iterative image reconstruction for CBCT using edge-preserving prior. Med Phys 2009;36:252-60.
76. Feldkamp LA, Davis LC, Kress JW. Practical cone-beam algorithm. J Opt Soc Am A 1984;1:612-9.
77. Wang G, Zhao S, Heuscher D. A knowledge-based cone-beam x-ray CT algorithm for dynamic volumetric cardiac imaging. Med Phys 2002;29:1807-22.
78. Jaffray DA, Siewerdsen JH, Wong JW, et al. Flat-panel cone-beam computed tomography for image-guided radiation therapy. Int J Radiat Oncol Biol Phys 2002;53:1337-49.
79. Purdie TG, Bissonnette JP, Franks K, et al. Cone-beam computed tomography for on-line image guidance of lung stereotactic radiotherapy: localization, verification, and intrafraction tumor position. Int J Radiat Oncol Biol Phys 2007;68:243-52.
80. Guckenberger M, Meyer J, Wilbert J, et al. Cone-beam CT based image-guidance for extracranial stereotactic radiotherapy of intrapulmonary tumors. Acta Oncol 2006;45:897-906.
81. Sonke JJ, Zijp L, Remeijer P, et al. Respiratory correlated cone beam CT.

Med Phys 2005;32:1176-86.
82. Li T, Xing L, Munro P, et al. Four-dimensional cone-beam computed tomography using an on-board imager. Med Phys 2006;33:3825-33.
83. Dietrich L, Jetter S, Tücking T, et al. Linac-integrated 4D cone beam CT: first experimental results. Phys Med Biol 2006;51:2939-52.
84. Thompson BP, Hugo GD. Quality and accuracy of cone beam computed tomography gated by active breathing control. Med Phys 2008;35:5595-608.
85. Boda-Heggemann J, Fleckenstein J, Lohr F, et al. Multiple breath-hold CBCT for online image guided radiotherapy of lung tumors: simulation with a dynamic phantom and first patient data. Radiother Oncol 2011;98:309-16.
86. Glide-Hurst CK, Ionascu D, Berbeco R, et al. Coupling surface cameras with on-board fluoroscopy: a feasibility study. Med Phys 2011;38:2937-47.
87. Harada T, Shirato H, Ogura S, et al. Real-time tumor-tracking radiation therapy for lung carcinoma by the aid of insertion of a gold marker using bronchofiberscopy. Cancer 2002;95:1720-7.
88. Shimizu S, Shirato H, Ogura S, et al. Detection of lung tumor movement in real-time tumor-tracking radiotherapy. Int J Radiat Oncol Biol Phys 2001;51:304-10.
89. Shirato H, Shimizu S, Kitamura K, et al. Four-dimensional treatment planning and fluoroscopic real-time tumor tracking radiotherapy for moving tumor. Int J Radiat Oncol Biol Phys 2000;48:435-42.
90. Shirato H, Shimizu S, Kunieda T, et al. Physical aspects of a real-time tumor-tracking system for gated radiotherapy. Int J Radiat Oncol Biol Phys 2000;48:1187-95.
91. Onimaru R, Fujino M, Yamazaki K, et al. Steep dose-response relationship for stage I non-small-cell lung cancer using hypofractionated high-dose irradiation by real-time tumor-tracking radiotherapy. Int J Radiat Oncol Biol Phys 2008;70:374-81.
92. Shirato H, Oita M, Fujita K, et al. Feasibility of synchronization of real-time tumor-tracking radiotherapy and intensity-modulated radiotherapy from viewpoint of excessive dose from fluoroscopy. Int J Radiat Oncol Biol Phys 2004;60:335-41.
93. Seppenwoolde Y, Berbeco RI, Nishioka S, et al. Accuracy of tumor motion compensation algorithm from a robotic respiratory tracking system: a simulation study. Med Phys 2007;34:2774-84.
94. Lu XQ, Shanmugham LN, Mahadevan A, et al. Organ deformation and dose coverage in robotic respiratory-tracking radiotherapy. Int J Radiat Oncol Biol Phys 2008;71:281-9.
95. Kupelian P, Willoughby T, Mahadevan A, et al. Multi-institutional clinical experience with the Calypso System in localization and continuous, real-time monitoring of the prostate gland during external radiotherapy. Int J Radiat Oncol Biol Phys 2007;67:1088-98.
96. Mayse ML, Parikh PJ, Lechleiter KM, et al. Bronchoscopic implantation of a novel wireless electromagnetic transponder in the canine lung: a feasibility study. Int J Radiat Oncol Biol Phys 2008;72:93-8.
97. Lechleiter K, Chaudhari A, Malinowski K, et al. SU-FF-J-75: the effect of time on inter-transponder distance implanted in lung: an initial study in a canine mode. Med Phys 2007;34:2385.
98. Cook A. FDA grants calypso medical IDE approval for pivotal lung cancer study. 2011.
99. Kupelian PA, Forbes A, Willoughby TR, et al. Implantation and stability of metallic fiducials within pulmonary lesions. Int J Radiat Oncol Biol Phys 2007;69:777-85.
100. Gierga DP, Brewer J, Sharp GC, et al. The correlation between internal and external markers for abdominal tumors: implications for respiratory gating. Int J Radiat Oncol Biol Phys 2005;61:1551-8.
101. Ionascu D, Jiang SB, Nishioka S, et al. Internal-external correlation investigations of respiratory induced motion of lung tumors. Med Phys 2007;34:3893-903.
102. Glide-Hurst CK, Schwenker Smith M, Ajlouni M, et al. Evaluation of two synchronized external surrogates for 4D CT sorting. J Appl Clin Med Phys 2013;14:4301.
103. Willoughby T, Lehmann J, Bencomo JA, et al. Quality assurance for nonradiographic radiotherapy localization and positioning systems: report of Task Group 147. Med Phys 2012;39:1728-47.
104. Yan H, Zhu G, Yang J, et al. The investigation on the location effect of external markers in respiratory-gated radiotherapy. J Appl Clin Med Phys 2008;9:2758.
105. Gianoli C, Riboldi M, Spadea MF, et al. A multiple points method for 4D CT image sorting. Med Phys 2011;38:656-67.
106. Schaerer J, Fassi A, Riboldi M, et al. Multi-dimensional respiratory motion tracking from markerless optical surface imaging based on deformable mesh registration. Phys Med Biol 2012;57:357-73.
107. Li R, Lewis JH, Cerviño LI, et al. 4D CT sorting based on patient internal anatomy. Phys Med Biol 2009;54:4821-33.
108. Yan D, Vicini F, Wong J, et al. Adaptive radiation therapy. Phys Med Biol 1997;42:123-32.
109. Yan D, Wong J, Vicini F, et al. Adaptive modification of treatment planning to minimize the deleterious effects of treatment setup errors. Int J Radiat Oncol Biol Phys 1997;38:197-206.
110. Yan D, Ziaja E, Jaffray D, et al. The use of adaptive radiation therapy to reduce setup error: a prospective clinical study. Int J Radiat Oncol Biol Phys 1998;41:715-20.
111. Sonke JJ, Belderbos J. Adaptive radiotherapy for lung cancer. Semin Radiat Oncol 2010;20:94-106.
112. Wulf J, Hädinger U, Oppitz U, et al. Stereotactic radiotherapy of extracranial targets: CT-simulation and accuracy of treatment in the stereotactic body frame. Radiother Oncol 2000;57:225-36.
113. Chang J, Mageras GS, Yorke E, et al. Observation of interfractional variations in lung tumor position using respiratory gated and ungated megavoltage cone-beam computed tomography. Int J Radiat Oncol Biol Phys 2007;67:1548-58.
114. Sonke JJ, Lebesque J, van Herk M. Variability of four-dimensional computed tomography patient models. Int J Radiat Oncol Biol Phys 2008;70:590-8.

115. Glide-Hurst CK, Gopan E, Hugo GD. Anatomic and pathologic variability during radiotherapy for a hybrid active breath-hold gating technique. Int J Radiat Oncol Biol Phys 2010;77:910-7.
116. Cohade C, Wahl RL. Applications of positron emission tomography/computed tomography image fusion in clinical positron emission tomography-clinical use, interpretation methods, diagnostic improvements. Semin Nucl Med 2003;33:228-37.
117. Woodford C, Yartsev S, Dar AR, et al. Adaptive radiotherapy planning on decreasing gross tumor volumes as seen on megavoltage computed tomography images. Int J Radiat Oncol Biol Phys 2007;69:1316-22.
118. Kupelian PA, Ramsey C, Meeks SL, et al. Serial megavoltage CT imaging during external beam radiotherapy for non-small-cell lung cancer: observations on tumor regression during treatment. Int J Radiat Oncol Biol Phys 2005;63:1024-8.
119. Haasbeek CJ, Lagerwaard FJ, Cuijpers JP, et al. Is adaptive treatment planning required for stereotactic radiotherapy of stage I non-small-cell lung cancer? Int J Radiat Oncol Biol Phys 2007;67:1370-4.
120. Wen N, Glide-Hurst C, Nurushev T, et al. Evaluation of the deformation and corresponding dosimetric implications in prostate cancer treatment. Phys Med Biol 2012;57:5361-79.
121. de la Zerda A, Armbruster B, Xing L. Formulating adaptive radiation therapy (ART) treatment planning into a closed-loop control framework. Phys Med Biol 2007;52:4137-53.
122. Li XA, Liu F, Tai A, et al. Development of an online adaptive solution to account for inter- and intra-fractional variations. Radiother Oncol 2011;100:370-4.
123. Men C, Jia X, Jiang SB. GPU-based ultra-fast direct aperture optimization for online adaptive radiation therapy. Phys Med Biol 2010;55:4309-19.
124. Men C, Gu X, Choi D, et al. GPU-based ultrafast IMRT plan optimization. Phys Med Biol 2009;54:6565-73.
125. Pratx G, Xing L. GPU computing in medical physics: a review. Med Phys 2011;38:2685-97.
126. Hugo G, Olsen K, Ford J, et al. WE-C-WAB-03: Correspondence Between FDG-PET and Diffusion-Weighted MRI After Deformable Registration in Locally-Advanced Non-Small Cell Lung Cancer. Med Phys 2013;40:477.
127. Ohno Y, Koyama H, Yoshikawa T, et al. Diffusion-weighted MRI versus 18F-FDG PET/CT: performance as predictors of tumor treatment response and patient survival in patients with non-small cell lung cancer receiving chemoradiotherapy. AJR Am J Roentgenol 2012;198:75-82.
128. Sukumar UK, Bhushan B, Dubey P, et al. Emerging applications of nanoparticles for lung cancer diagnosis and therapy. Int Nano Lett 2013;3:45.
129. Holgersson G, Bergström S, Ekman S, et al. Radiosensitizing biological modifiers enhancing efficacy in non-small-cell lung cancer treated with radiotherapy. Lung Cancer Management 2013;2:251-5.

Cite this article as: Glide-Hurst CK, Chetty IJ. Improving radiotherapy planning, delivery accuracy, and normal tissue sparing using cutting edge technologies. J Thorac Dis 2014;6(4):303-318. doi: 10.3978/j.issn.2072-1439.2013.11.10